Multifunctionalization of wool fabrics through nanoparticles: a chemical route towards smart textiles

Multifunctionalization of wool fabrics through nanoparticles: A chemical route towards smart textiles

Stefania Mura [a,⇑], Gianfranco Greppi [a,b], Luca Malfatti [c], Barbara Lasio [c], Vanna Sanna [d], Maria Elena Mura [e],Salvatore Marceddu [f], Antonella Lugliè [b]

[a] Nucleo di Ricerca sulla Desertificazione, Università degli Studi di Sassari, Viale Italia 39, 07100 Sassari, Italy

[b] DADU, Dipartimento di Architettura Design e Urbanistica, Università degli Studi di Sassari, Palazzo del Pou Salit, Piazza Duomo 6, 07041 Alghero, SS, Italy

[c] Laboratorio di Scienza dei Materiali e Nanotecnologie, CR-INSTM, Università di Sassari, Palazzo Pou Salit, Piazza Duomo 6, 07041 Alghero, SS, Italy

[d] Department of Chemistry and Pharmacy, Laboratory of Nanomedicine, University of Sassari, c/o Porto Conte Ricerche, Tramariglio, 07041 Alghero, SS, Italy

[e] Bioecopest srl, Technology Park of Sardinia, Loc. Tramariglio, 07041 Alghero, SS, Italy

[f] CNR – Istituto Scienze delle Produzioni Alimentari Traversa La Crucca, 3 – Località Baldinca, 07040 Li Punti, Sassari, Italy

1. Introduction

Wool is a widely used biomaterial mainly composed of fibrous proteins that are insoluble and tough, such as keratins [1]. These filaments of keratins are aligned in the fiber axis constituting macrofibrils with diameter around 300 nm that are covered by a lipid membrane and linked by a intermacrofibrillar matrix called cell membrane complex (CMC). The fiber formation is due to the peptide bonds that facilitate the alignment of cysteine, allowing the formation of disulfide cross-links that give thermal stability and rigidity to these materials. Although their excellent physical properties as biological materials, wool fibers suffer the disadvantage of being photosensitive to UV, having bad sweat venting properties, and scarce water absorption [2]. This feature, in particular limits their use by affecting the dyeing, the finishing and the wear- ing comfort of the fabrics; hydrophobicity, in fact, can create dis- comfort to people for its static charge on wool tissues. A second major disadvantage in the use of wool is the tendency to sheltering microorganisms providing good energy source of nutrients for their growth. This generally causes fiber damages and skin irritations [3], especially in the case of garments and carpets [4]. Loading antimicrobials is therefore of capital importance for the production of advanced hygienic and medical textiles based on wool. Up to now, despite different approaches have been explored to improve the hydrophilic properties of wool fabrics, the use of nanotechnology seems a promising route for mastering the surface properties of this biomaterial. Nanotechnology, in fact, enables a smart functionalization of the biofibers providing new features such as antibacterial activity, photo-degradation and self cleaning. Nanomaterials, and in particular nanoparticles (NPs), are able to use incident light to decompose dirt, stains and microorganisms through photocatalysis, and protect tissues against UV degradation, fulfilling the needs for innovation in the fields of garments, carpets and building materials.

In previous years, the wool functionalization was carried out through a single type of nanoparticle having a specific chemical composition, such as silver (Ag) and silica (SiO_2) or titania (TiO_2). Some research groups used Ag NPs to improve the colour strength of fabrics and their antibacterial properties. In these studies, how- ever, the Ag NPs where directly used, without embedding the particles in specific polymers [5,6]. This approach has some drawbacks as NPs-modified garments, for instance, can lead to a human skin irritation or damage. Furthermore, some of these studies used a not-environmental friendly method that exploited toxic reducing agents for the synthesis of AgNPs, such as sodium borohydride $NaBH_4$ [3,5], butylamine ($ButNH_2$) [6], sodium hypophosphite (SHP) [7], sodium dithionite and sodium bisulfite [8].

Silica NPs were often added to wool fiber in order to obtain a superhydrophilic fabric by modifying the surface roughness, the sur- face energy and the water absorption of wool [9]. This type of approach is interesting because the degree of hydrophobicity of the wool seems to be controlled by the density and the size of the NPs.

Finally, the functionalization with TiO_2 NPs was used with the aim to improve the UV protection of the fibers and the photocatalytic properties [10,11]. The self cleaning properties of modified wool with TiO_2 were also described by Daoud et al. [2] and Behzadnia et al. [12], and its effect against the photoyellowing was demonstrated by Zhang et al. [13]. The functionalization with this type of NPs, however, causes a decrease in the tensile proper- ties of the wool fibers. More recently, a high efficiency in stain removal, antibacterial and superhydrophilic properties of the wool fibers were obtained by using a combination of Ag with TiO_2 or SiO_2 NPs, and TiO_2/SiO_2 nanocomposite [7,14,15]. To the best of our knowledge, however, the combination of three different NPs and the possible effects on wool fabrics was not reported yet.

In the present work self-cleaning, UV-resistance, hydrophilicity, and antibacterial properties of the wool were explored by anchor- ing TiO_2, SiO_2 and Ag NPs to the fabrics. In addition, we tried to design new multifunctional textiles through the combination of the three different NPs, taking the advantages of their specific properties. This approach can be important because the functional properties of every single material could benefit of the combined functionalization.

2. Materials and methods

2.1. Reagents

Tetraethyl orthosilicate (TEOS) (98%, Aldrich), ethanol (99.99%, Aldrich), and ammonium hydroxide (30%, Aldrich) were used with- out any further purification. Milli-Q water (18.2 Ω) was used throughout the experiment. 100% of untreated wool fabric was purchased from La robbia (Sardinia) and used as substrate. Titanium isopropoxide (TIP, 97%) and absolute ethanol were pur- chased from Sigma–Aldrich (Germany). $AgNO_3$ solution (99.9%), Glacial acetic acid, Methylene Blue, Alginic acid sodium salt, LB agar were purchased by Aldrich, Germany. The chemicals were used as received.

Escherichia coli (*E. coli* ATCC 11299) was chosen as typical microorganism.

2.2. Synthesis of nanoparticles

2.2.1. Synthesis of silica NPs

The SiO_2 particles were obtained by hydrolysis of tetraethyl orthosilicate (TEOS) in ethanol. TEOS (3 mL) was added drop by drop to a solution of EtOH (50 mL), ammonium hydroxide (30% w/v, mL) and water (1 mL) and left under shaking for 5 h. After 48 h at room temperature (25 °C) the white suspension was centrifuged at 13,000 rpm for 10′ with different washing steps to eliminate the solvents. Then, the NPs were collected and dispersed in 100 mL of water to a 0.05 M final concentration.

2.2.2. Synthesis of titania NPs

TiO_2 NPs were prepared by an alcohothermal method without the use of any specific organic reagent. The Titanium isopropoxide (TIP) precursor was added dropwise into a stirred mixture containing water and ethanol (TIP/water/ethanol volume ratio 3:4:90 v/v). After sonication for 1 h, the crystallization of TiO_2 was achieved in a mitten at 180 °C for 24 h. The obtained TiO_2 NPs were collected by centrifugation and then resuspended in water to a 0.01 M final concentration.

2.2.3. Synthesis of alginate capped AgNPs (AlgnAg NPs) composite

Alginate capped Ag NPs were synthesized by adding 2 mL of freshly prepared 1 10^{-2} M $AgNO_3$ solution to 50 mL of 0.2% (w/v) alginate solution, with constant stirring at 90 °C. The obtained solution was diluted to 100 mL with a final 0.01 M con- centration. A brown color of the solution indicated the formation of Ag NPs.

2.3. Characterization of nanoparticles

The formation of Ag NPs was monitored by UV–Vis spectroscopic measurements with a spectrophotometer (Cary 3E UV–visible, Varian).

Morphological examination of NPs was performed by environ- mental scanning electron microscopy (ESEM) (Zeiss LS10, Germany). A drop of NPs aqueous suspension was deposited on aluminum stub and dried until complete water evaporation. The samples were then analyzed at 20 kV acceleration voltage after gold sputtering (Sputter Coater Edwards S150A), under an argon atmosphere.

The X-ray diffraction (XRD) pattern of the as-obtained particles was obtained by using Cu Kα radiation (k = 0.154056 nm), with a Bruker D8 Discover diffractometer in grazing incidence geometry; the X-ray generator worked at a power of 40 kV and 40 mA with the angle of 2h ranging from 10° to 100° at a scan speed of 0.5 deg/min and an increment of 0.02°. Water suspensions were deposited on a

silicon wafer and dried at open air. The crystallite size of the nanoparticles was determined by the Scherrer equation $D = K\lambda/\beta \cos\theta$, where D is the diameter of the particle, λ is the X-ray wavelength, β is the full width at half-maximum (fwhm) of the diffraction line, θ is the diffraction angle, and K is a constant, 0.89. Particle size (PS) and polydispersity index (PdI) were measured using dynamic light scattering (DLS) (Nanosizer S90 particle size analyzer; Malvern Instruments, UK) at a temperature of 25 °C, and a scattering angle of 90°, after dilution of NPs with Milli-Q water. Each sample was measured in triplicate.

2.4. Preparation of wool fabrics

Wool fabrics of 2X2 cm dimension and woolen threads 3 cm long, were prepared and purified by washing in acetone for 20', in an ultrasonic bath, to remove the impurities. Samples were taken out and then dried at 40 °C [5]. The wool fabrics were immersed for 10' at RT in NP solutions adjusted to pH 3.0 with acetic acid. The following NPs solutions were used: TiO_2 NPs (indicated as T), SiO_2 NPs (S), Ag NPs (A), the combination of NPs with a ratio 1:1 v/v of TiO_2 and SiO_2 (TS), SiO_2 and Ag NPs (SA), TiO_2 and Ag NPs (TA) and, finally, a combination of TiO_2, SiO_2 and Ag NPs with a ratio 1:1:1 v/v (TSA). The wool samples immersed in these solutions were put in a oven at 80 °C for 30', extracted by the solutions, washed with distilled water and then dried in a oven at 80 °C.

2.5. Analysis of wool fabrics

2.5.1. SEM and XRF analysis

The morphology of the wool sample treated with TSA solution was examined by SEM analysis as previously described. X-ray Fluorescence (XRF) spectrometry was used for the analysis of the wool samples (pristine or functionalized with NPs). This is an analytical technique based on X-rays for the chemical characterization of the samples and for the detection of the elements constituent the material. The analysis was carried out by a μ-XRF technique with a Bruker M4 Tornado spectrometer using a Rh anode X-ray source model MCBM 50–0.6 B working at 50 kV and 600 A under vacuum (20 mbar) with an Al filter 12.5 μm thick. Elemental map- ping for the sample of wool with Ag nanoparticles was focused on an area of the size of 2.74×mm x 0.78 mm and the map was obtained through the integration of 10 different measurements for 30 min of acquisition. For the analysis the individual wool fibers were focused by the microscope inside the instrument with the objectives 10 and 100 to detect the elements. To verify the absorption of NPs in wool samples XRF measurements were carried out to discriminate peaks related to Ag, Ti and Si. The quantification of elemental composition was realized applying a semi-automatic method by using the software M4 Tornado. The weight percentage (wt.%) and atomic percentage (at.%) of the elements was utilized to estimate the relative amount of loaded NPs onto or into the wool fabric.

2.5.2. *Study of antibacterial activity*

E. coli (ATCC 11299), a gram negative bacterium which causes urinary tract and wound infections [12], was used as a popular test organism in AATCC 100-2004 (clause 10.2) test method [7]. The bacterial inocula were prepared to obtain a bacterial suspension in exponential growth of 10^8 colony forming units (CFU) mL^{-1} in a nutrient broth (Luria Bertani Broth). Antibacterial tests were car- ried out on untreated wool fabrics, used as control, and on wool fabrics modified with TiO_2, SiO_2 and Ag NPs. Wool wires 3 cm long were sterilized in autoclave, and each sample was placed in a conical flask with 2 mL of LB and 1 mL of inoculum ($1x10^5$ cells) and left O/N at 37 °C in agitation. Then 1 mL of inoculum was diluted with 49 mL of sterile water and left in agitation for 30'. Finally 1 mL of the last dilution was taken and further diluted with 9 mL

of fresh sterile water. This procedure was repeated for further 5 times to obtain 6 dilutions. From each dilution 100 lL were taken and plated on LB agar. So a series of diluted solutions 1:10 were prepared, plated and incubated at 37 °C O/N. After incubation the number of colonies was counted to compare treated and untreated samples. Three technical replicates were carried out. Finally the antimicrobial activities of raw and treated samples against *E. coli* were calculated by counting the colony-forming-units (CFU) and it was checked that the dilution factor was respected. The percent- age of bacteria reduction by the fabric treatment was calculated as follows:

$$R\% = [(A\ B)/A]\ 100,$$

where A = numbers of bacteria colonies recovered from the untreated wool; B = numbers of bacteria colo- nies recovered from the treated wool after inoculation and incubation, and (R) is the reduction percentage of bacteria colonies.

Another test was carried out to verify the antibacterial activity, incubating 9 mL of LB with 1 mL of *E. coli* inoculum (1×10^5 cells) and lefting in agitation O/N at 37 °C. One test tube was left without wool as control while the others were incubated with the modified wool. When the *E. coli* sample reached an OD of 0.5 (exponential growth phase), the absorbance measurements of the solutions containing the wool samples were carried out at the spectrophotometer (Cary 3E UV–visible, Varian) at a wavelength of 600 nm and theresults were compared with the sample without wool.

2.5.3. *Contact angle analysis*

The wettability of the wool samples was evaluated by contact angle analysis (Dataphysics OCA 20), after the deposition of a drop of water (5 µL) on the pristine or wool samples impregnated with NPs and estimating the angle between an ideal horizontal plane,

supporting the surface of the droplet, and the drop. The contact angle was taken as a median of at least 3 measurements.

2.5.4. *Discoloration of methylene blue*

Photocatalytic performance of TiO_2 NPs was studied by degra- dation of methylene blue (MB). 200 µL

of a MB solution (0.01 g/50 mL) were deposited on a wool sample and dried at room conditions. Than the self-cleaning function was assessed based on the degradation of MB stain from the fabrics placed at ambient temperature (25 °C) under natural daylight irradiation in Sardinia (November) for two consecutive days. Photocatalytic activity and self cleaning properties of the material were monitored by a color variation.

3. Results and discussion

3.1. Characterization of NPs

SiO_2 nanoparticles were prepared using a sol–gel process based on a modified Stober method [16] because of their easy and green preparation. In this way monodisperse SiO_2 nanoparticles with a narrow size distribution, can be obtained from aqueous alcohol solutions of silicon alkoxides (TEOS) in the presence of ammonium hydroxide as a catalyst. The NPs size depends on the type of silicon alkoxide and alcohol that are used in the synthesis while the

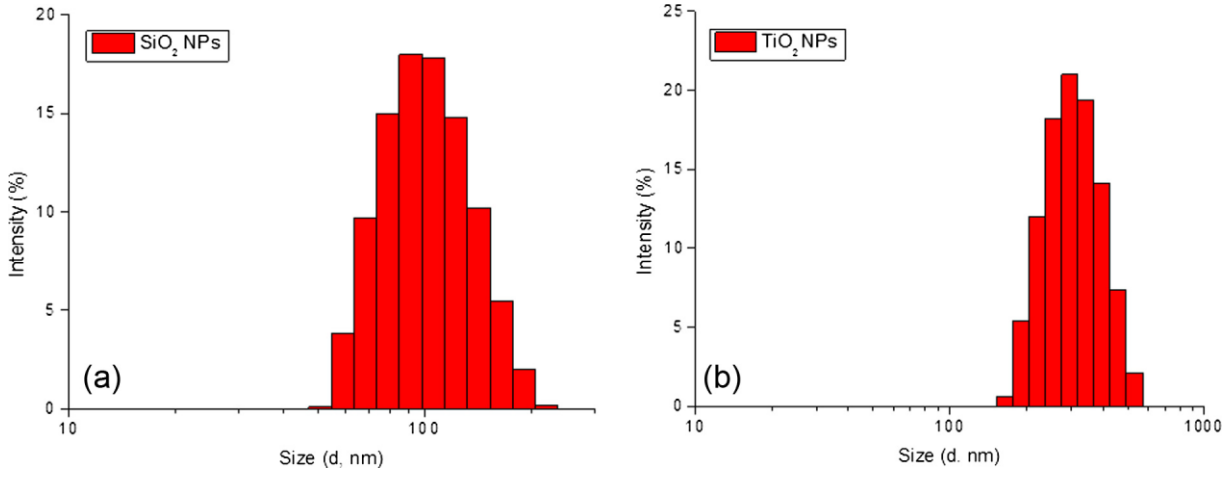

Fig. 1. Size distribution of SiO_2 NPs (a) and TiO_2 NPs (b) obtained by DLS.

reaction conditions (the concentration of TEOS, ammonia and water, the concentration of alcohol and the reaction temperature) influence the condensation rate and the formation of a 3D network or a single layer composed of monodisperse particles [17]; for this reason a particular attention is necessary during the preparation ofthese NPs with a constant monitoring of these conditions.

As reported in Fig. 1a, the SiO_2 NPs showed a mean diameter of 102.9 ± 0.4 nm, and are characterized by an unimodal distribution,as confirmed by PdI values of 0.173 ± 0.006.

TiO_2 NPs were synthesized using a two steps technique that uses ultrasounds combined with a

solvothermal method. The pre- sent synthesis is based on a modified alcohothermal method by Hu et al. [18] for the sonosynthesis of titania NPs, avoiding the use of toxic organic agents. These NPs presented high photocatalytic activity, that was evidenced by self cleaning properties, due to the good crystallinity of the material that produces a good separation of photoinduced charges. Ultrasound-chemistry, in fact, is an environmentally friendly and efficient approach that requires low temperature and short time for the synthesis [12]. Ultrasounds consist of rare fraction and compression cycles that create cavitation bubbles that can collapse and generate regions with high temperature and pressure that act as microreactors that transform the energy of sound into a chemical reaction. Furthermore these waves increase the velocity of collision among particles, avoiding the formation of larger particles.

Through XRD analysis the crystalline structure of TiO_2 NPs was assessed. Fig. 2a shows the XRD pattern of TiO_2 sample that revealed the formation of a broad peak at 25.31° that corresponds to the anatase crystalline structure of titanium dioxide [14] obtained through the one-step alcohotermal reaction. The crys- talline structure of the as-obtained solid particles is indexed by comparing the standard peaks of anatase phase [10]. The XRD anal- ysis of TiO_2 NPs in fact reveals the formation of anatase peaks at 25.31° (101), 37.8° (004), 48.0° (200), 54.3° (105), 56° (211), 63.2° (204), 68.8° (116), 70° (220), 75° (215) of the pattern that belong to the plans of the crystals of anatase, and are in agreement with the data list in JCPDS Card No. 21-1272 [10]. Also, the peaks at 44.24° and 64.73°, related to rutile phase of nano titania, are visi- ble, so these NPs should impart a photocatalytic property to mate- rials in which they are embedded. The crystallite size of the TiO_2 NPs was calculated with Scherrer's equation and was around 8 nm. Through the full width at half maximum of peaks (FWHM), the crystal sizes can be compared to DLS analysis. The results indicated that the particle mean diameter is 260.6 ± 2.40 nm (Fig. 1b), and the NP dispersions shows a PdI values of 0.222 ± 0.01 which is typical of monodispersed systems. By comparing the DLS results with those of XRD, we argue that the TiO_2 NPs are made of small monocrystalline titania clusters that merged during the sonochemical synthesis.

The synthesis of Ag NPs is typically based on the reduction of a silver salt in presence of a stabilizer, that prevents the aggregation of NPs. The chemical reductants that are normally used included sodium borohydride, hydrazine, dimethylformamide and stabilizers as polyaniline (PANI) and polyvinylpyrrolidone (PVP) [19,20]. All these compounds are generally associated with biological and environmental risks due to their toxicity and non biocompatibility. Therefore it is important to use an ecofriendly method for synthesizing NPs. In the present work we modified the method by Sharma

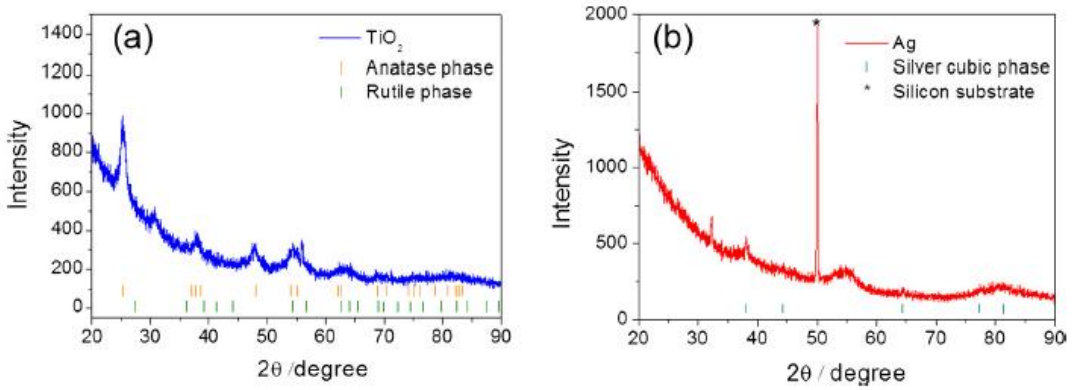

Fig. 2. XRD pattern of TiO_2 NPs (a) and Alg–Ag NPs (b).

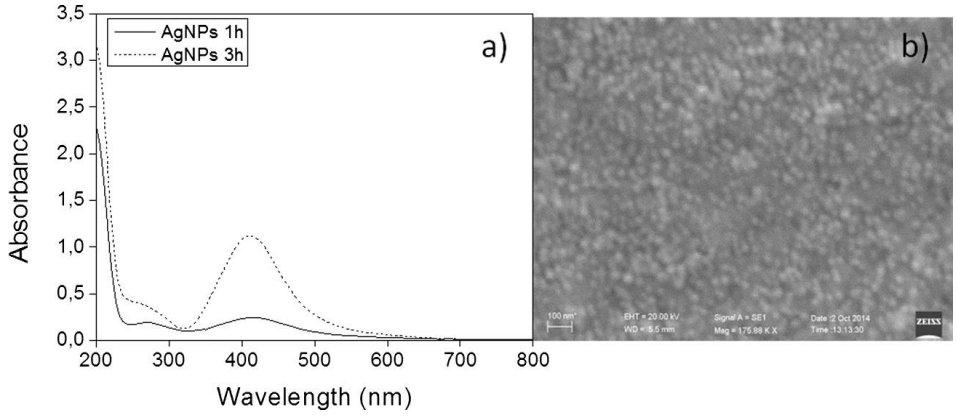

Fig. 3. UV–Vis spectra of Ag NPs at different time of reaction (a) and SEM image of Ag NPs (b) after 3 h of reaction (dimension bar: 100 nm).

et al. [19], that makes use of a natural carbohydrate based biopolymer (alginate) as template, to produce Ag NPs with an excellent biocompatibility. Alginate, in fact, is a natural polysaccharide derived from brown marine algae, it is cheap, biocompatible and is an environmental benign biopolymer used as non-toxic food additive and in food industry. Alginate produces a chelation of Ag^+ by the adjacent hydroxyl and carboxylic groups of polymer [17] and, after heating, the Ag^+ chelate produces Ag^0. This synthesis allows to obtain Ag NPs reproducibly and without interfering impurities. As illustrated in Fig. 3a, the UV–vis spectroscopy revealed the formation, after 1 h of reaction, of a peak at 413 nm, characteristic of plasmon resonance of Ag NPs. To complete the reaction it was necessary to continue the reaction for

other 2 h. As it is evident from the upper curve, the intensity of the peak increased as the concentration of Ag NPs increased with time till it became constant after 3 h.

The peak obtained was symmetric and sharp, indicating a nar- row size distribution of Ag NPs. SEM analysis (Fig. 3b) showed that the Ag NPs were well-dispersed, with a spherical shape and a mean diameter around 20 nm. The crystalline phase and size of the Ag NPs were confirmed by XRD and results are reported in Fig. 2b. The defined diffraction peaks at 38.3°, 44.2° and 64.5°, correspond- ing to (111), (200) and (220) planes of the cubic crystal structure (fcc) of Ag metal (JCPDS No. 65-2871) can be clearly identified in the spectrum [20]. An intense peak due to the Si substrate at 50° and to alginate at 32° are also present. Furthermore, the average crystallite size calculated through the Scherrer equation was about 23 nm, confirming the SEM measurements.

3.2. Characterization of functionalized wool fabrics

Wool fibers, consisting of a protein, keratin, are abundant in amino and carboxyl groups, so the charge of the surface is related to the pH [9]. When the pH of the solution is around 4 different amino groups of the wool fiber are protonated, leading to the fiber a positive surface charge that allows to react with negative charged agents, as dyes or NPs, that can be loaded on wool by electrostatic interaction. The functionalization of wool with TiO_2, SiO_2 and Ag NPs was carried out through electrostatic interactions and in this way multifunctional fabrics were obtained. In fact at low pH the wool fibers contain just few anionic groups and NPs have a sufficient charge to maintain their stability and dispersion. It seems that the CMC and other low sulfur regions are the route of entry of chemicals [5].

Herein, the wool fibers were functionalized by using different combination of NPs and characterized by XRF measurements and SEM analyses. From Table 1 is clear that the main elements of wool fibers are S and Ca, while Cl, K, and Fe are present with a minor amount. Considering the loading of TiO_2 into wool samples, the best results were obtained in samples where titania is alone. The

Table 1

The quantitative XRF elemental analysis of wool samples, without and with different nanoparticles, expressed as wt.%/at.%.

Sample (wt.%/at.%)	Wool	Titania T	Silica S	TSA
S	36.13/41.63	33.53/39.92	33.19/37.57	60.28/64.59
Cl	0	1.70/1.83	2.38/2.44	3.48/3.37
K	1.63/1.5	0.24/0.23	0.42/0.39	0.36/0.32

	4			
Ca	60.21/55.51	42.45/40.44	59.34/53.74	24.01/20.59
Fe	0.67/0.44	0.27/0.19	0.25/0.17	0.31/0.19
Zn	0.86/0.49	Nd	Nd	Nd
Ti	Nd	21.81/17.39	Nd	6.25/4.49
Si	Nd	Nd	4.41/5.70	5.26/6.44
Ag	Nd	Nd	Nd	0.05/0.02

loading of SiO_2 to the wool sample is more effective when a com- bination with other NPs was used, as in the case of TSA sample.

The analysis, however, did not allow verifying the Ag NPs load- ing in wool samples; this is likely due to the small size of the Ag nanoparticles, that are not aggregated because of their surface coating. Therefore a larger area of wool functionalized with Ag NPs was mapped (SI Fig. S1) by XRF, looking specifically for the Ag signal. The fiber shows a homogeneous elemental distribution of Ag on the sample (SI Fig. S1, yellow color).

The surface morphology of a wool sample covered with a com- bination of TiO_2/SiO_2/Ag NPs was analyzed through SEM at different magnifications. As shown in Fig. 4, the surface of wool fibers is smooth with scales; the coating with NPs does not have a negative effect on the morphology of the native wool fiber, and this coating is not perceptible to the touch of the fiber.

As illustrated in Fig. 4a–c, the wool sample shows scales on the fiber surface and the NPs are disposed on the whole wool surface, but predominantly are inserted into the creeks (Fig. 4d), almost forming a pocket of NPs. In particular in Fig. 4e is possible to see the different NPs into the pocket and to determine their distribution by their particle size. These NPs are supposed to be SiO_2 NPs (around 100 nm, Fig. 4e and f), present in higher concentration, composed of several aggregated particles, while on the wool surface TiO_2 NPs (around 200 nm, Fig. 4e) and Ag NPs (around 20 nm, Fig. 4e and f) can be observed. These NPs are condensed as a layer on the fibers, and confer roughness to the material. The average particle size of NPs estimated by SEM is similar to DLS measurements and to the crystallite size calculated through Scherrer's equation.

3.3. Antibacterial properties of functionalized wool fabrics

The antibacterial activity of modified wool was measured against *E. coli*. Fabrics treated with NPs presented antibacterial

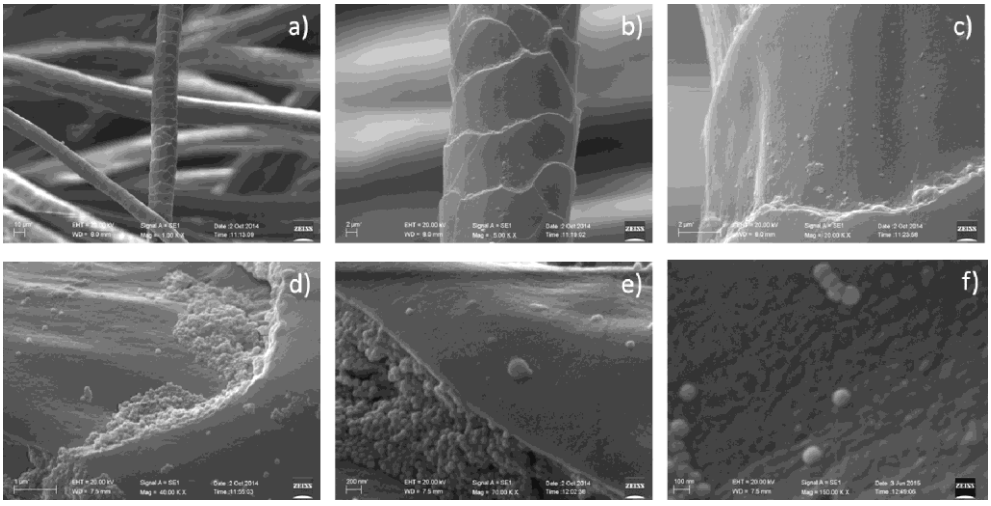

Fig. 4. SEM images of wool functionalized with TiO_2/SiO_2/Ag NPs (TSA) at different magnification (dimensional bar: 10 µm (a), 2 µm (b) and (c), 1 µm (d), 200 nm (e) and 100 nm (f)).

features as illustrated in Fig. 5a where a good reduction of the number of colonies was observed for samples treated with Ag NPs alone (A), while a minor reduction was observed for samples with Ag NPs in combination (TA and SA). The maximum inhibition of bacterial growth was observed for TSA samples, that are the fibers functionalized with the most diluted solutions of NPs (ratio 1:1:1 v/v).

It is important to point out that all the samples were impregnated with the same volume of NPs solution. This means that the concentration of Ag NPs in the solution used for the functionalization of the sample A is the triple of that in the solution used for the preparation of the sample TSA. Keeping in mind the synthetic pro- tocol, we can argue that the main contribution of the antibacterial activity is due to Ag NPs. Nevertheless, the synergic activity of Ag, SiO_2 and TiO_2 allows reaching a better performance, providing an antibacterial activity which is higher than pure Ag NPs alone.

The reduction of CFU was calculated, after counting the number of colonies in petri dishes, to describe the antibacterial efficiency of the treated samples through the reduction rate percentage (SI Fig. S2) that for TSA sample was equal to 72%. As result the bacterial reduction due to Ag NPs was excellent against *E. coli*, considering that only a wire of 3 cm inhibited the growth of a very high number of bacteria and that

the inhibition depends by Ag NPs con- centration. The huge reduction of colonies due to AgNPs is also evident at naked eye by looking at the agar plates. In Fig. 5b in fact the plates from solutions treated with only wool and wool with TS are shown in comparison to those prepared from solutions after the treatment with Ag, and TSA NPs.

As expected, Ag NPs are very effective in inhibiting the growth of bacteria, however, more interestingly, an antimicrobial effect was also observed for samples treated with a combination of the three types of NPs providing an excellent activity even at low con- centration of nanoparticles.

3.4. Contact angle measurements

Although wool is a hydrophobic material, it is possible to modify its surface and its wettability to improve the comfortableness of the fabric [15,21–24]. With this purpose wool was modified with nanoparticles and the wettability of the fibers was studied through water contact angle measurements by casting a water droplet on the wool and monitoring the angle variations with time. Immediately after casting, the water droplets deposited on untreated wool (W, Fig. 6) shows a contact angle of 164°. This value is comparable to the angle obtained from wool with SiO_2 NPs (S) while an initial angle of 154° was found for wool with TiO_2, SiO_2 and Ag NPs (TSA).

After 2 s from casting, however, a big difference of contact angle was observed; the wool functionalized with three different NPs (TSA_1) showed a contact angle that is almost 0 °C, while the wool functionalized with silica NPs continue showing a similar contact angle value (144°). In the untreated wool used as reference the

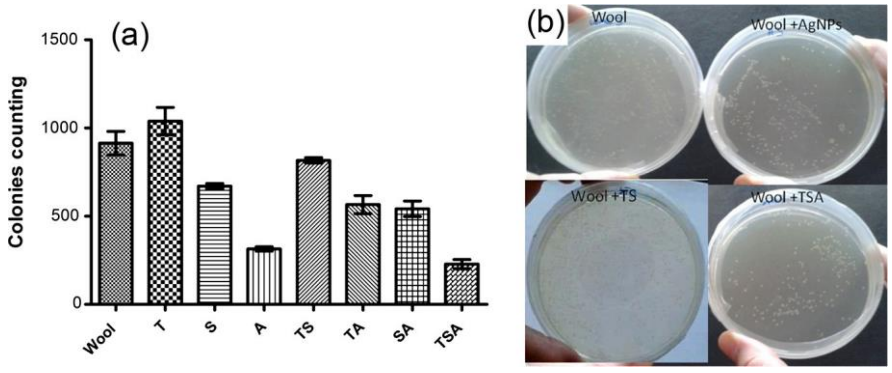

Fig. 5. Colonies counting on petri dishes (a) and images of plates with *E. coli* (b) after treatment of the solutions with pristine wool and wool treated with Ag, TS, and TSA NPs.

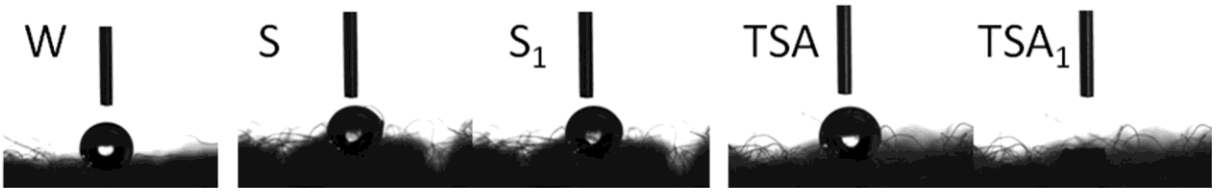

Fig. 6. Dynamic contact angle measurements on pristine wool (W) and on treated wool as deposited (S and TSA) and 2 s after drop deposition (S1 and TSA1).

droplet shape remains constant up to several minutes as for samples treated with only titania (TiO_2). In fact the use of titania alone increases the wool hydrophobicity (not shown in figure). These experiments prove that the simultaneous inclusion of TiO_2, SiO_2 and Ag NPs into wool, with the concentrations used, changed the fabric to be superhydrophilic. In previous works [3] this was demonstrated for wool with included SiO_2 NPs while in this experiment the best results were obtained with the combination of three different NPs. In fact as demonstrated from XRF measurements (Table 1), a greater loading of SiO_2 NPs in the wool fabric was obtained by a combination of 3 different NPs and not with only SiO_2 NPs. To explain the possible mechanism for the superhydrophilicity of the modified wool fabrics, we can hypothesize a capillary penetration of water when it is placed on the hydrophilic nanoparticles and then a subsequent water transfer through the fabric. In fact, the inclusion of the NPs in wool fabrics led to an increase of surface energy and wettability. The wettability is the force that drives the penetration and depends on the surface energy and roughness of the material. The NPs inclusion in wool fabrics efficiently improve the surface roughness (that cannot be perceived by touching the fibers) in fact a layer of nano-protuberances with a spherical shape can be observed by SEM images on the fiber surface. It is important to underline that an increase in the NPs sizes, and a consequent increase of the sur- face/volume ratio, could weakened the interactions between wool and NPs, resulting in a decreased coverage of the fibers. NPs with small diameter, such as Ag NPs, increase the roughness of the fabric and play a fundamental role for the fabrication of superhydrophilic wool fabrics, as previously reported [6,8].

The surface energy of not-treated wool fibers is low, due to the presence on the outer layer of fatty acids that confers hydrophobicity to the material. The addition of silica and titania particles in combination increases the surface energy because of the presence of Si–OH and Ti–OH groups, and at certain concentrations allows tuning the fabrics wettability.

3.5. Self cleaning properties

The self cleaning property of the modified wool samples was verified through the removal of MB stain on fabrics after one day of daylight irradiation, using the UV of natural sun to induce the photocatalytic properties of titania to decompose stains. UV illumi- nation triggers the photocatalytic activity of titania that is excited under UV. SI Fig. S3 illustrates the discoloration of MB on wool samples before (up) and after one day of daylight irradiation (down). The best result of discoloration was obtained for the sample T and TS, while the sample TSA keeps a quite strong blue stain. In both samples T and TS the stain removal is due to nanocrystalline anatase that modifies the stains and produces the colorless degraded product. When silica is used in combination with titanium dioxide particles, the interaction between titania active sites and dye molecules are stronger [14,21], due to the increase of the surface area near titanium dioxide and, the surface acidity of the photocatalyst, causes a good decomposition rate, as observed in TS sample. In fact the silica NPs are smaller than the titania particles and play efficiently the role of ‘‘spacers’’ among the photocatalytic NPs; in the absence of titania, the dye decomposition was not observed.

As demonstrated in a previous study [25], the temperature largely affects the photocatalytic properties of titania. In particular, in the range between 38 and 100 °C, the kinetics of the organic degradation is strongly enhanced, as shown for the decomposition of Pluronic F127 deposited on photocatalytic titania films [26]. Considering the wool substrates and their applications for clothing, carpets, garments and building materials, we can hypothesize that an excursion from 20 to 45 °C could further enhance the self cleaning properties of the smart textiles.

4. Conclusions and future outlook

This study shows a simple, new and environmental friendly method to obtain superhydrophilic, antibacterial and partially self-cleaning wool fabrics through a functionalization with SiO_2, Ag and TiO_2 NPs. The obtained wool fabrics functionalized with silver NPs presented an antibacterial activity against *E. coli*. The best antimicrobial activity and superhydrophilicity was found for the combination of the three NPs, property improved by the presence of silica NPs. This is the first study that provided the combination of three different NPs and we obtained the best results from this combination for antimicrobic and superhydrophilic properties.

Further work is required to test the durability of the tissues to washing cycles for possible application in garments, carpets and materials for building.

Inorganic NPs have unique physico-chemical characteristics which have been exploited in many biomedical applications (imaging, cell tracking and drug delivery) and lately also in personal care products, cosmetics and clothing [27–31]. In recent years there is an increasing need to understand nanomaterial tissue interactions at cellular and systemic levels, not only to optimize the therapeutic applications but also to minimize potential side effects [32–34]. In this context, the potential dermal or

systemic toxicity of TiO_2, SiO_2, and Ag NPs after topical exposure has been extensively explored [35–40]. From available *in vitro* and *in vivo* studies, it is reasonable to conclude that under normal use conditions on healthy skin, the NPs penetration pose minimal health concern [41–49].

Furthermore, considering that all studies imply greater exposure than any existing release of NPs from wool, we can assume that the use of modified wool in real life (clothing, garments, carpets and building materials) should not cause cell damages and be considered biocompatible. However, the evaluation of toxicity related to the effective absorption through the skin of all the three NPs released from the wool tissues, provide a significant opportunity for further investigative studies.

Acknowledgments

This project was financed by Legge 7, Regione autonoma della Sardegna, a grant of the master & back program. Thanks to La Robbia for the wool provided and a particular thanks to zia Pinuccia Sechi for the knitting and preparation of wool samples.

References

[1] P. Fortier, S. Suei, L. Kreplak, PLoS ONE 7 (7) (2012).
[2] W.A. Daoud, S.K. Leung, W.S. Tung, J.H. Xin, K. Cheuk, K. Qi, Chem. Mater. 20 (4) (2008) 1242–1244.
[3] B. Tang, J. Wang, S. Xu, T. Afrin, W. Xu, L. Sun, X. Wang, J. Colloid Interface Sci. 356 (2) (2011) 513–518.
[4] H. Barani, M. Montazer, N. Samadi, T. Toliyat, Colloids Surf., B 92 (2012) 9–15.
[5] R. Perumalraj, Int. Scholarly Res. Network ISRN Chem. Eng. (2012) 1–4.
[6] I. Osório, R. Igreja, R. Franco, J. Cortez, Mater. Lett. 75 (2012) 200–203.
[7] M. Montazer, A. Behzadnia, E. Pakdel, M.K. Rahimi, M.B. Moghadam, J. Photochem. Photobiol. B – Biol. 103 (3) (2011) 207–214.
[8] M. Hosseinkhani, M. Montazer, S. Eskandarnejad, M.K. Rahimi, Colloids Surf., A 415 (2012) 431–438.
[9] D. Chen, L. Tan, H. Liu, J. Hu, Y. Li, F. Tang, Langmuir 26 (7) (2010) 4675–4679. [10] H. Zhang, H. Yan, N. Mao, Ind. Eng. Chem. Res. 53 (5) (2014) 2030–2041.
[11] A. Nazari, M. Montazer, M. Dehghani-Zahedani, Ind. Eng. Chem. Res. 52 (3) (2013) 1365–1371.
[12] A. Behzadnia, M. Montazer, A. Rashidi, M.M. Rad, Ultrason. Sonochem. 21 (5) (2014) 1815–1826.
[13] H. Zhang, K.R. Millington, X. Wang, Polym. Degrad. Stab. 94 (2) (2009) 278–283.
[14] E. Pakdel, W.A. Daoud, X. Wang, Appl. Surf. Sci. 275 (2013) 397–402.
[15] B. Tang, J. Wang, S. Xu, T. Afrin, J. Tao, W. Xu, L. Sun, X. Wang, Chem. Eng. J. 185–186 (2012) 366–373.
[16] W. Stober, A. Fink, E. Bohn, J. Colloid Interface Sci. 26 (1968) 62–69.
[17] K.S. Rao, K. El-Hami, T. Kodaki, K. Matsushige, K. Makino, J. Colloid Interface Sci. 289 (1) (2005) 125–131.
[18] C. Hu, T. Lu, F. Chen, R. Zhang, C. Lian, S. Zheng, Q. Hu, S. Duo, Mater. Res. Bull. 53 (2014) 42–48.
[19] S. Sharma, P. Sanpui, A. Chattopadhyay, S.S. Ghosh, RSC Adv. 2 (2012) 5837– 5843 (The Royal Society of Chemistry).
[20] X. Lü, S. Cui, Bioresour. Technol. 101 (12) (2010) 4703–4707.
[21] W.S. Tung, W.A. Daoud, Acta Biomater. 5 (1) (2009) 50–56.

[22] F.A. Sadr, M. Montazer, Ultrason. Sonochem. 21 (2) (2014) 681–691.
[23] M. Montazer, E. Pakdel, J. Photochem. Photobiol. C – Photochem. Rev. 12 (4) (2011) 293–303.
[24] L. Rintoul, E.A. Carter, S.D. Stewart, P.M. Fredericks, Biopolym. – Biospectrosc. Sect. 57 (1) (2000) 19–28.
[25] Q. Hu, B. Liu, Z. Zhang, M. Song, X. Zhao, J. Wuhan Univ. Technol. – Mater. Sci. Ed. 25 (2010) 210–213.
[26] S. Costacurta, G. Dal Maso, R. Gallo, M. Guglielmi, G. Brusatin, P. Falcaro, ACS Appl. Mater. Interfaces (2010) 1294–1298, http://dx.doi.org/10.1021/ am100149.
[27] L. Yildirimer, N.T. Thanh, M. Loizidou, A.M. Seifalian, Nano Today (2011) 585– 607.
[28] R. Cheng, F. Feng, F. Meng, C. Deng, J. Feijen, Z. Zhong, J. Controlled Release 152 (2011) 2–12, http://dx.doi.org/10.1016/j.jconrel.2011.01.030.
[29] C. Huang, K.G. Neoh, L. Wang, E.T. Kang, B. Shuter, Contrast Media Mol. Imaging (2011) 298–307, http://dx.doi.org/10.1002/cmmi.427.
[30] J. Pan, D. Wan, J. Gong, Chem. Commun. (2011) 3442–3444, http://dx.doi.org/ 10.1039/c0cc05520 (Camb).
[31] N.T.K. Thanh, B. Raton (Eds.), Magnetic Nanoparticles: From Fabrication to Clinical Applications, CRC Press/Taylor and Francis, 2011.
[32] S.M. Hussain, K.L. Hess, J.M. Gearhart, K.T. Geiss, J.J. Schlager, Toxicol. In Vitro (2005) 975–983.
[33] S.J. Kang, B.M. Kim, Y.J. Lee, H.W. Chung, Environ. Mol. Mutagen. (2008) 399– 405, http://dx.doi.org/10.1002/em.20399.
[34] T. Xia, M. Kovochich, J. Brant, M. Hotze, J. Sempf, T. Oberley, C. Sioutas, J.I. Yeh, M.R. Wiesner, A.E. Nel, Nano Lett. (2006) 1794–1807.
[35] P.J. Lu, W.L. Cheng, S.C. Huang, Y.P. Chen, H.K. Chou, H.F. Cheng, Int. J. Cosmet. Sci. (2015), http://dx.doi.org/10.1111/ics.12239.
[36] C.N. Miller, N. Newall, S.E. Kapp, G. Lewin, L. Karimi, K. Carville, T. Gliddon, N.M. Santamaria, Wound Repair Regen. (2010) 359–367, http://dx.doi.org/ 10.1111/j.1524-475X.2010.00603.
[37] X. Chen, H.J. Schluesener, Toxicol. Lett. (2008) 1–12.
[38] D.M. Eby, H.R. Luckarift, G.R. Johnson, ACS Appl. Mater. Interfaces (2009) 1553–1560, http://dx.doi.org/10.1021/am9002155.
[39] J. Liao, M. Anchun, Z. Zhu, Y. Quan, Int. J. Nanomed. (2010) 337–342.
[40] Z. Lu, J. Xiao, Y. Wang, M. Meng, J. Colloid Interface Sci. (2015) 8–14, http:// dx.doi.org/10.1016/j.jcis.2015.04.015.
[41] W.G. Reifenrath, E.M. Chellquist, E.A. Shipwash, W.W. Jederberg, Fundam. Appl. Toxicol. (1984) S224–S230.
[42] J. Lademann, H. Weigmann, C. Rickmeyer, H. Barthelmes, H. Schaefer, G. Mueller, W. Sterry, Skin Pharmacol. Appl. Skin. Physiol. (1999) 247–256.
[43] C. Bennat, C.C. Müller-Goymann, Int. J. Cosmet. Sci. (2000) 271–283, http:// dx.doi.org/10.1046/j.1467-2494.2000.00009.
[44] A. Mavon, C. Miquel, O. Lejeune, B. Payre, P. Moretto, Skin Pharmacol. Physiol. (2007) 10–20.
[45] H. Nabeshi, T. Yoshikawa, K. Matsuyama, Y. Nakazato, A. Arimori, M. Isobe, S. Tochigi, S. Kondoh, T. Hirai, T. Akase, T. Yamashita, K. Yamashita, T. Yoshida, K. Nagano, Y. Abe, Y. Yoshioka, H. Kamada, T. Imazawa, N. Itoh, S. Tsunoda, Y. Tsutsumi, Pharmazie (2010) 199–201.
[46] W. Lin, Y.W. Huang, X.D. Zhou, Y. Ma, Toxicol. Appl. Pharmacol. (2006) 252– 259.
[47] H. Yang, C. Liu, D. Yang, H. Zhang, Z. Xi, J. Appl. Toxicol. (2009) 69–78, http:// dx.doi.org/10.1002/jat.1385.
[48] M. Chen, A. von Mikecz, Exp. Cell Res. (2005) 51–62.
[49] D. Lison, L.C. Thomassen, V. Rabolli, L. Gonzalez, D. Napierska, J.W. Seo, M. Kirsch-Volders, P. Hoet, C.E. Kirschhock, J.A. Martens, Toxicol. Sci. (2008) 155– 162, http://dx.doi.org/10.1093/toxsci/kfn072